

REPORT

QUANTUM SIMULATION

Observation of a prethermal discrete time crystal

A. Kyprianidis^{1,*†}, F. Machado^{2,3†}, W. Morong¹, P. Becker¹, K. S. Collins¹, D. V. Else⁴, L. Feng¹, P. W. Hess⁵, C. Nayak^{6,7}, G. Pagano⁸, N. Y. Yao^{2,3}, C. Monroe¹

Extending the framework of statistical physics to the nonequilibrium setting has led to the discovery of previously unidentified phases of matter, often catalyzed by periodic driving. However, preventing the runaway heating that is associated with driving a strongly interacting quantum system remains a challenge in the investigation of these newly discovered phases. In this work, we utilize a trapped-ion quantum simulator to observe the signatures of a nonequilibrium driven phase without disorder—the prethermal discrete time crystal. Here, the heating problem is circumvented not by disorder-induced many-body localization, but rather by high-frequency driving, which leads to an expansive time window where nonequilibrium phases can emerge. Floquet prethermalization is thus presented as a general strategy for creating, stabilizing, and studying intrinsically out-of-equilibrium phases of matter.

The periodic modulation of a system represents a versatile technique for controlling its behavior, which enables the emergence of phenomena ranging from parametric synchronization to dynamic stabilization (1). Periodic driving has become a staple in fields from nuclear magnetic resonance spectroscopy to quantum information processing (2–4). On a more fundamental level, the periodic Floquet drive also imbues a system with a discrete time-translational symmetry. Notably, this symmetry can be utilized to protect newly discovered Floquet topological phases or spontaneously broken to form time-crystalline order (5–15).

The realization of many-body Floquet phases of matter requires overcoming two crucial challenges. First, the system must not absorb energy from the driving field. In the presence of a periodic drive, dynamics are not constrained by energy conservation, and Floquet heating causes a generic many-body system to approach infinite temperature, which precludes the existence of any nontrivial order (16). Second, genuine late-time dynamics must be clearly differentiated from early-time transient behavior: A phase of matter can only be characterized after dynamical processes lead to the steady state behavior.

The conventional strategy for addressing the first (heating) challenge is to utilize strong disorder to induce many-body localization (MBL), where the presence of an extensive set of conserved local quantities prevents Floquet heating (17). However, requiring MBL leads to its own set of challenges, including stringent constraints on both the dimensionality and the range of interactions (18, 19). Moreover, the presence of strong disorder further slows down equilibration, making it even more difficult to overcome the second (time scale) challenge and distinguish between early- and late-time dynamics. Notably, long-lived subharmonic responses, characteristic of time-crystalline order, have also been observed in certain superfluid quantum gases without disorder (13, 20–22); the absence of Floquet heating in such systems is a result of an effective few-body description of the quantum dynamics (23).

Recently, an alternate, disorder-free framework for addressing both these challenges has emerged—Floquet prethermalization (24–28). For sufficiently high Floquet drive frequencies, energy absorption by the many-body system requires multiple correlated local rearrangements, strongly suppressing the heating rate. The Floquet heating time τ^* scales exponentially with the drive frequency and can thus be prolonged beyond experimentally practical time scales. For time $t < \tau^*$, the system dynamics are captured by an effective prethermal Hamiltonian H_{eff} (24, 25). This prethermal Hamiltonian defines an effective energy for the Floquet system and also determines the nature of the prethermal state, which is reached at the much shorter local equilibration time τ_{pre} . Thus, by focusing on times between τ_{pre} and τ^* , the dynamics are guaranteed to reflect the actual thermodynamic properties of the Floquet phase.

This intermediate prethermal regime need not be trivial: Additional symmetries, protected

by the discrete time-translation symmetry of the drive, can emerge and lead to intrinsically nonequilibrium phases of matter (29, 30). One example of such a phase is the prethermal discrete time crystal (PDTC), in which the many-body system spontaneously breaks the discrete time-translation symmetry of the drive and develops a robust subharmonic response.

A disorder-free PDTC exhibits a number of key differences compared with the MBL discrete time crystal, despite the similarity of their subharmonic responses (23, 31). When stabilized by MBL, time-crystalline order is independent of the initial state and persists to arbitrarily late times but is believed to only occur in low dimensions with sufficiently short-range interactions (18, 19). By contrast, the PDTC lifetime is limited by τ^* and depends on the energy density of the initial state; this energy density determines the prethermal state to which the system equilibrates for times $t > \tau_{\text{pre}}$. Crucially, if the prethermal state spontaneously breaks the emergent symmetry of H_{eff} , the many-body system also exhibits robust time-crystalline order, corresponding to an oscillation between the different symmetry sectors (29, 30). On the other hand, if the prethermal state is symmetry-unbroken, the system will be in a trivial Floquet phase with any signatures of time-crystalline order decaying by τ_{pre} . The requirement of a symmetry-broken phase further distinguishes the PDTC and its MBL counterpart and highlights the PDTC's stability in higher dimensions. In one dimension, Landau-Peierls arguments rule out the existence of a PDTC with short-range interactions (32), and long-range interactions are necessary to stabilize a prethermal time crystal (30).

We exploit the controlled long-range spin-spin interactions of an ion trap quantum simulator to observe signatures of a one-dimensional prethermal discrete time crystal. Our main results are threefold. First, we prepare a variety of locally inhomogeneous initial states through the individual addressing of ions within the one-dimensional chain (Fig. 1A). By characterizing the quench dynamics starting from these states, we directly observe the approach to the prethermal state, which enables the experimental extraction of the prethermal equilibration time, τ_{pre} . Second, we measure the time dynamics of the energy density as a function of the driving frequency. By preparing states near both the bottom and the top of the spectrum (Fig. 1B), we observe either the gain or loss of energy as the system heats to infinite temperature (corresponding to zero energy density). Notably, we find that the heating time scale, τ^* , increases with the driving frequency (Fig. 2). Finally, to probe the nature of prethermal time-crystalline order, we study the Floquet dynamics of different initial states that equilibrate to either a symmetry-broken or a symmetry-unbroken ensemble. The former

¹Joint Quantum Institute, Department of Physics, and Joint Center for Quantum Information and Computer Science, University of Maryland, College Park, MD 20742, USA.

²Department of Physics, University of California, Berkeley, CA 94720, USA. ³Materials Sciences Division, Lawrence Berkeley National Laboratory, Berkeley, CA 94720, USA.

⁴Department of Physics, Massachusetts Institute of Technology, Cambridge, MA 02139, USA. ⁵Department of Physics, Middlebury College, Middlebury, VT 05753, USA.

⁶Microsoft Quantum, Station Q, Santa Barbara, CA 93106, USA. ⁷Department of Physics, University of California, Santa Barbara, CA 93106, USA. ⁸Department of Physics and Astronomy, Rice University, Houston, TX 77005, USA.

*Corresponding author. Email: akyprian@umd.edu

†These authors contributed equally to this work.

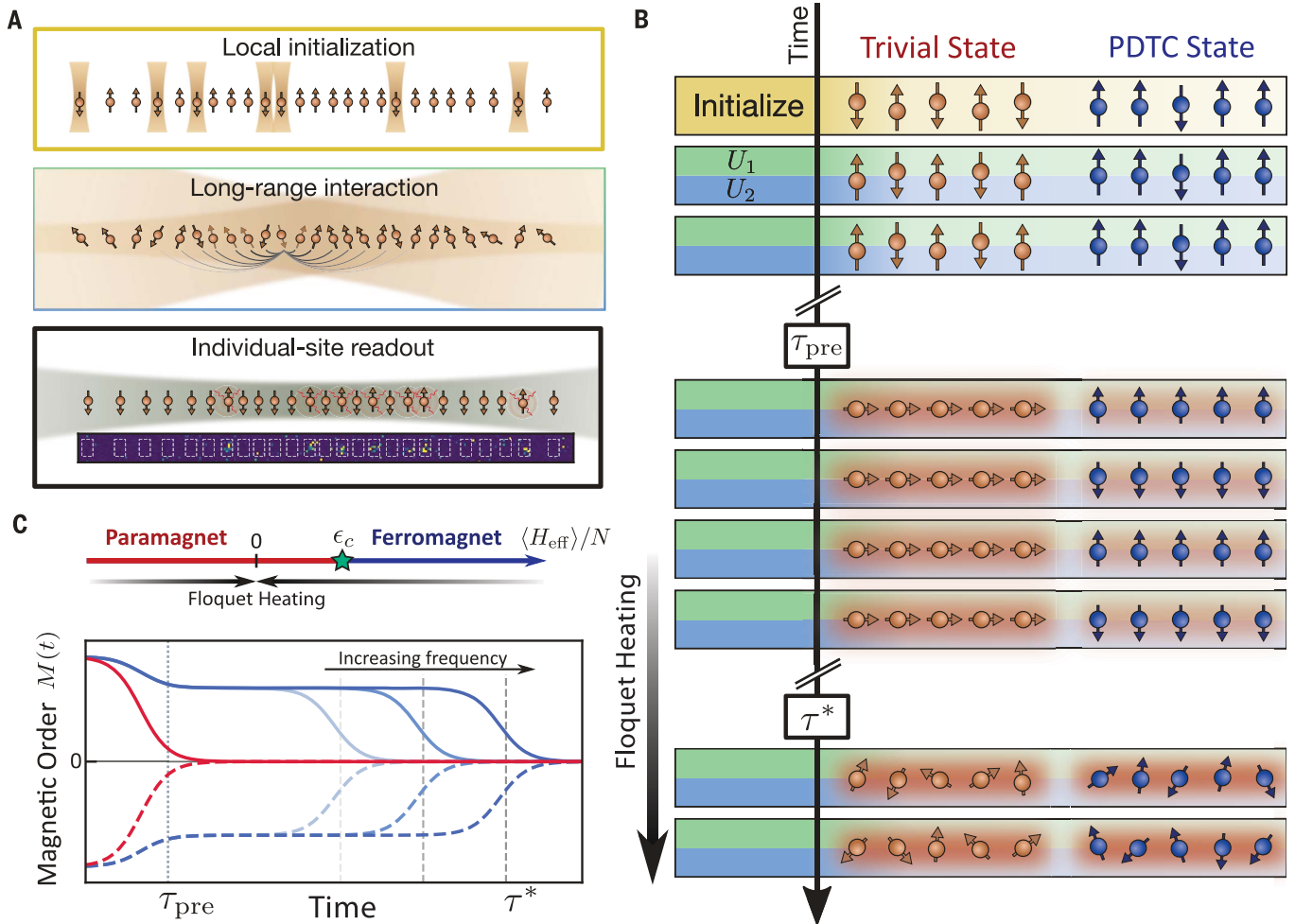


Fig. 1. Experimental setup and protocol. (A) Schematic of the 25-ion chain (35). Single-site addressing (top), global Raman beams (middle), and state-dependent fluorescence (bottom) enable the preparation, evolution, and detection of the quantum dynamics. (B) For intermediate times ($\tau_{\text{pre}} < t < \tau^*$), the system approaches an equilibrium state of the prethermal Hamiltonian H_{eff} . In the trivial Floquet phase, the magnetization after τ_{pre} decays to zero. In the PDTC phase, the magnetization changes sign every period, which leads to a robust subharmonic response. At times $t \gg \tau^*$, Floquet heating brings the many-

body system to a featureless infinite temperature ensemble. (C) (Top) Phase diagram of H_{eff} . Owing to the antiferromagnetic nature of the Ising interactions $J_{ij} > 0$, the ferromagnetic phase occurs at the top of the many-body spectrum. (Bottom) Schematic of the stroboscopic magnetization dynamics in the trivial (red) and PDTC (blue) phase (full and dashed curves represent even and odd driving periods, respectively). When the energy density of the initial state is above the critical value ϵ_c , the system is in the PDTC phase, and its lifetime follows the frequency-dependent heating time τ^* .

exhibits robust period-doubling behavior up until the frequency-controlled heating time scale, τ^* (Fig. 3B). In comparison, for the latter, all signatures of period doubling disappear by the frequency-independent time scale τ_{pre} (Fig. 3A). By investigating the lifetime of the time-crystalline order as a function of the energy density of the initial state, we identify the phase boundary for the PDTC.

Our system consists of a one-dimensional chain of 25 $^{171}\text{Yb}^+$ ions. Each ion encodes an effective spin-1/2 degree of freedom in its hyperfine levels $|F=0, m_F=0\rangle$ and $|F=1, m_F=0\rangle$ (Fig. 1A). Long-range Ising interactions are generated through a pair of Raman laser beams (33, 34). Arbitrary effective magnetic fields can be applied either locally or globally and single-site readout can be performed

simultaneously across the full chain (35), enabling the direct measurement of the Floquet dynamics of both the magnetization and the energy density.

The Floquet drive alternates between two types of Hamiltonian dynamics (Fig. 1B): (i) a global π -pulse around the \hat{y} axis and (ii) an evolution for time T under a disorder-free, long-range, mixed-field Ising model. This is described by the two evolution operators

$$U_1 = \exp \left[-i \frac{\pi}{2} \sum_i \sigma_i^y \right]$$

$$U_2 = \exp \left[-iT \left(\sum_{i<j} J_{ij} \sigma_i^x \sigma_j^x + B_y \sum_{i=1}^N \sigma_i^y + B_z \sum_{i=1}^N \sigma_i^z \right) \right] \quad (1)$$

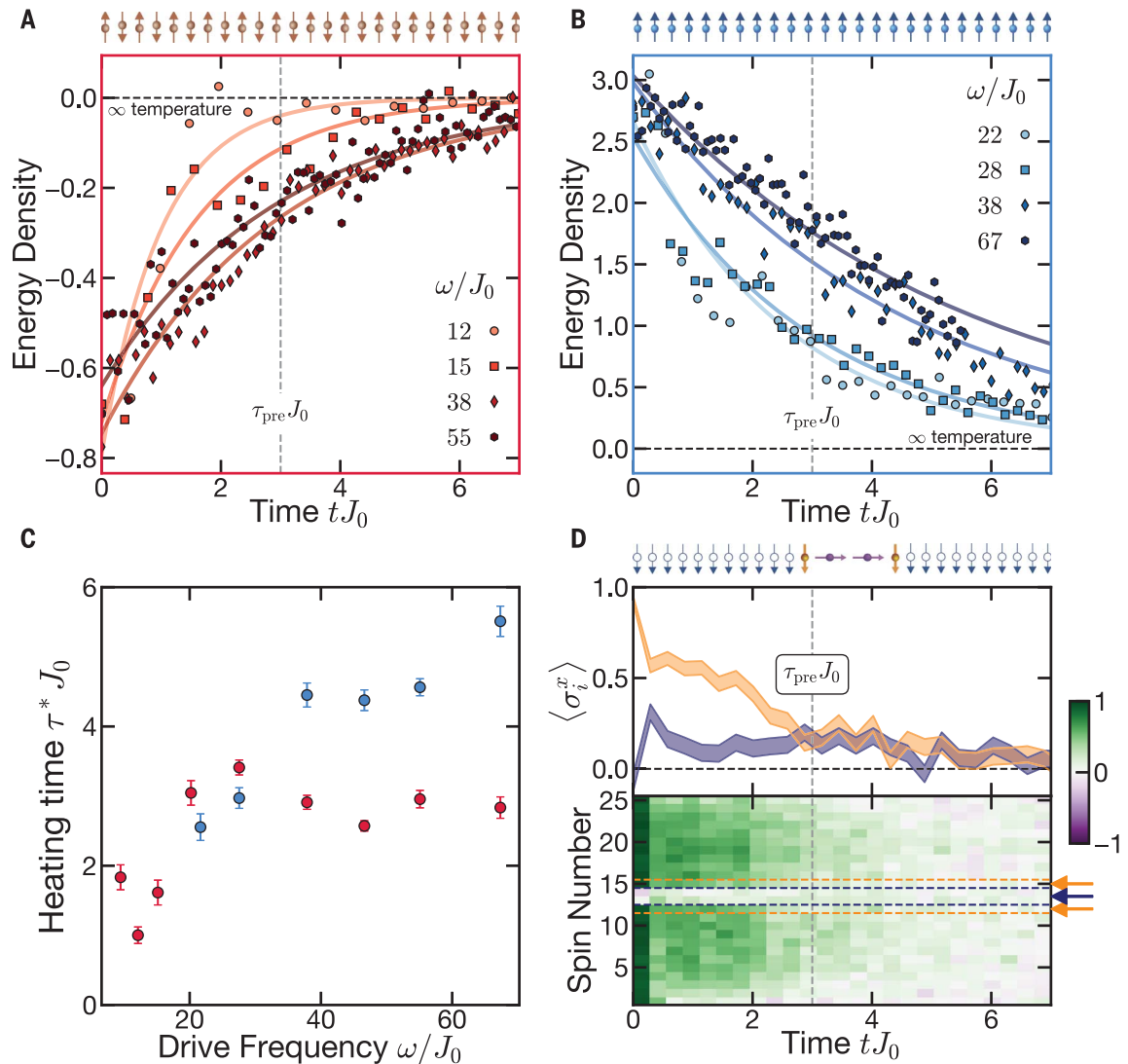
where σ_i^v is the v -th component of the spin-1/2 Pauli operator for the i -th ion, and we adopt the convention $\hbar = 1$. Here, $J_{ij} > 0$ is the long-range coupling with average nearest-neighbor interaction strength $J_0 = 2\pi \cdot 0.33$ kHz, whereas $B_y = 2\pi \cdot 0.5$ kHz and $B_z = 2\pi \cdot 0.2$ kHz are global effective magnetic fields. The Floquet unitary $U_F = U_2 U_1$ implements the dynamics over a period of the drive and has frequency $\omega = 2\pi/T$.

Within the prethermal window in time $\tau_{\text{pre}} < t < \tau^*$, the stroboscopic dynamics of the system (every other period) are well approximated by an effective prethermal Hamiltonian, which to lowest order in $1/\omega$ is given by (30)

$$H_{\text{eff}} = \sum_{i<j}^N J_{ij} \sigma_i^x \sigma_j^x + B_y \sum_{i=1}^N \sigma_i^y \quad (2)$$

Fig. 2. Characterizing the prethermal regime.

(A and B) The dynamics of the energy density for a low-energy Néel state (A) and a high-energy polarized state (B) highlights the frequency dependence of the heating rate. Statistical error bars are of similar size as the point markers. (C) Heating time τ^* for the Néel (red) and polarized (blue) states, extracted through an exponential fit ($\sim e^{-t/\tau^*}$) to the energy density dynamics [solid curves in (A) and (B)]. The presence of external noise leads to a saturation of τ^* at high frequencies. Error bars for the heating time correspond to fit errors. (D) Characterization of the prethermal equilibration time, τ_{pre} , via the local \hat{x} -magnetization dynamics for even Floquet periods. (Top) The middle two spins (purple), initially prepared along the \hat{z} axis, rapidly align with their neighbors (orange) at time $\tau_{\text{pre}} J_0 \approx 3$, signaling local equilibration to the prethermal state. The shaded bands represent the standard error of the mean. (Bottom) \hat{x} -magnetization dynamics across the entire ion chain.



A crucial feature of H_{eff} is that long-range Ising interactions stabilize a ferromagnetic phase along the \hat{x} axis. However, owing to the antiferromagnetic nature of the interactions ($J_{ij} > 0$), this phase does not occur at low energy density close to the bottom of the spectrum, but rather at high energy density near the top of the spectrum (Fig. 1C).

We begin by characterizing the dynamics of the system as it approaches the prethermal state of H_{eff} . In particular, we prepare an initial state with all spins pointing along \hat{x} (in an eigenstate of σ^x), except for two central spins, which are prepared along \hat{z} (Fig. 2D). Quench dynamics from this initial state show that the magnetization of the two central spins exhibits two-step dynamics. The \hat{x} -magnetization $\langle \sigma_i^x \rangle$, starting at zero, first equilibrates to the value of the neighboring spins before decaying back to zero at late times. The convergence of the initially inhomogeneous \hat{x} -magnetization

to a uniform finite value demonstrates that the system first reaches an intermediate-time equilibrium (i.e., prethermal) state before ultimately heating to infinite temperature. We find that this prethermal time scale is approximately given by $J_0 \tau_{\text{pre}} \approx 3$.

In addition to τ_{pre} , the prethermal regime is also characterized by the time scale associated with the frequency-dependent Floquet heating, τ^* . To experimentally investigate τ^* , we measure the dynamics of the prethermal energy density, $\langle H_{\text{eff}} \rangle / (NJ_0)$, for two different initial states on opposite ends of the many-body spectrum of H_{eff} : a low-energy Néel state (Fig. 2A) and a high-energy polarized state (Fig. 2B). In both cases, we observe the expected trend—increasing the driving frequency suppresses the heating rate (Fig. 2C). However, the finite decoherence time of the system (induced by external noise sources) sets an upper bound

on the maximum heating time scale; as a result, at large drive frequency, τ^* cannot grow exponentially with increasing drive frequency, but rather approaches a plateau value (34). Even in the presence of this decoherence dynamics, the separation between τ^* and τ_{pre} enables experimental access to the prethermal regime.

The demonstration of the frequency dependence of τ^* (Fig. 2) directly translates into our ability to control the lifetime of the prethermal time crystal. As previously mentioned, the key ingredient underlying time-crystalline order is the presence of an emergent symmetry, G , in H_{eff} , which is not a microscopic symmetry present in the Hamiltonian (Eq. 1), but rather a direct consequence of the periodic driving protocol (29, 30). In our experiment, this symmetry corresponds to a global spin flip, $G \approx U_1 \propto \prod_{i=1}^N \sigma_i^y$. Although G is not a symmetry of the original evolution (Eq. 1),

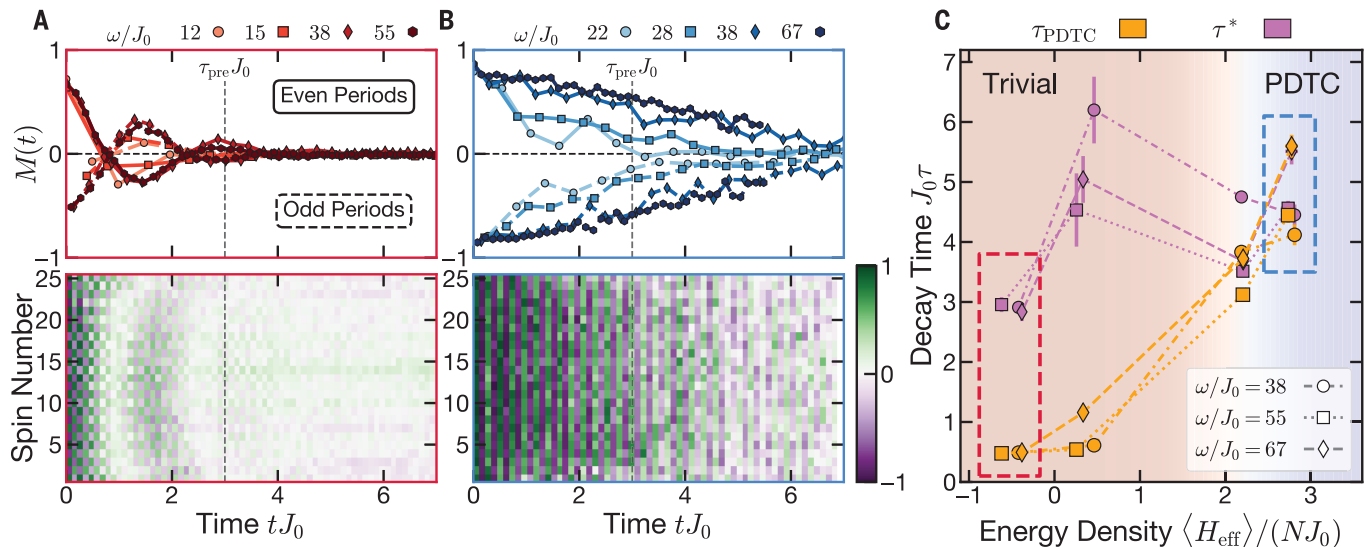


Fig. 3. Characterizing the PDTC phase. (A and B) (Top) Magnetization dynamics, $M(t)$, for the Néel state (A) and the polarized state (B). For the Néel state, $M(t)$ quickly decays to zero at time τ_{pre} (dashed vertical line), independent of the drive frequency. For the polarized state, the subharmonic response ($2T$ -periodicity) persists well beyond τ_{pre} , and its lifetime is extended upon increasing the drive frequency. The lifetime of the prethermal time-crystalline order τ_{PDTC} is obtained by fitting the magnetization dynamics to an exponential decay (34). Statistical error bars are of similar size as the point markers. (Bottom) $\dot{\chi}$ -magnetization dynamics across the entire ion chain at $\omega/J_0 = 38$. (C) Heating

(τ^*) and magnetization decay (τ_{PDTC}) times for four different initial states at varying energy densities (34). At low energy densities, τ_{PDTC} (orange) are substantially shorter than τ^* (magenta) and independent of frequency, highlighting the trivial Floquet phase. At high energies, τ_{PDTC} is similar to τ^* , highlighting the long-lived, frequency-controlled nature of the PDTC behavior. The location of the observed crossover in energy density is in agreement with an independent quantum Monte Carlo calculation (red and blue shaded regions) (34). Error bars for the decay time correspond to fit errors, whereas error bars for the energy density correspond to statistical errors.

it is present in H_{eff} (Eq. 2). When such emergent symmetry is present, the exact Floquet dynamics are approximately generated by evolving under H_{eff} for time T , followed by the action of G . This latter part suggests that the time-crystalline order is naturally captured by the system's magnetization dynamics; the action of G changes the sign of the order parameter $\langle \sigma_i^x \rangle$ every period. As a result, there are two possibilities for the prethermal dynamics, depending on the system's energy density (Fig. 1B). If the prethermal state corresponds to the symmetry-respecting paramagnet, the magnetization is zero and remains unchanged across a period. Conversely, if the prethermal state corresponds to the symmetry-breaking ferromagnet, the magnetization is nonzero and alternates every period. The resulting $2T$ -periodic, subharmonic dynamics is the hallmark of a time crystal.

We investigate these two regimes by measuring the autocorrelation of the magnetization

$$M(t) = \frac{1}{N} \sum_{i=1}^N \langle \sigma_i^x(t) \rangle \langle \sigma_i^x(0) \rangle \quad (3)$$

Starting with a low-energy density Néel state (Fig. 3A), we observe that $M(t)$ quickly decays to zero at τ_{pre} , in agreement with the expectation that the system equilibrates to the symmetry-unbroken, paramagnetic phase. This behavior is frequency-independent, in direct contrast to

the Floquet dynamics of the energy density (Fig. 2A). This contrast highlights an essential point: Although τ^* can be extended by increasing the driving frequency, no order survives beyond τ_{pre} when the system is in the trivial Floquet phase.

The Floquet dynamics starting from the polarized state are markedly distinct (Fig. 3B). First, $M(t)$ exhibits period doubling, with $M > 0$ for even periods and $M < 0$ for odd periods. Second, the decay of this period-doubling behavior is directly controlled by the frequency of the drive. Third, the lifetime of the time-crystalline order mirrors the dynamics of the energy density shown in Fig. 2B, demonstrating that Floquet heating ultimately melts the PDTC at late times.

By considering two additional initial states, we explore the stability of the PDTC phase as a function of energy density. Figure 3C depicts both the heating time and the lifetime of the time-crystalline order. Near the bottom of the spectrum, where no symmetry-breaking phase exists, the decay of the magnetization is frequency-independent and substantially faster than the heating time scale. By contrast, near the top of the spectrum, where a symmetry-breaking ferromagnetic phase exists, the two time scales are consistent with one another and thus Floquet heating limits the PDTC lifetime. Our results are consistent with a phase boundary occurring at energy density $\langle H_{\text{eff}} \rangle / (NJ_0) \approx 2$, in agreement with independent numerical calculations from quantum Monte Carlo (34).

In this work, we report the experimental observation of robust prethermal time-crystalline behavior that persists beyond any early-time transient dynamics. Our results highlight the potential of periodic driving, in general, and prethermalization, in particular, as a framework for realizing and studying out-of-equilibrium phenomena. Even in the presence of noise, we find that the prethermal dynamics remain stable, which suggests that an external bath at sufficiently low temperature can stabilize the prethermal dynamics for infinitely long times (29). This stands in contrast to localization-based approaches for stabilizing Floquet phases, in which the presence of an external bath tends to destabilize the dynamics. Our work points to a number of future directions: (i) exploring generalizations of Floquet prethermalization to a quasi-periodic drive (36), (ii) stabilizing Floquet topological phases (37, 38), and (iii) leveraging nonequilibrium many-body dynamics for enhanced metrology (39).

REFERENCES AND NOTES

1. L. D. Landau, E. M. Lifshitz, *Mechanics, Third Edition: Course of Theoretical Physics, Volume 1* (Butterworth-Heinemann, ed. 3, 1976).
2. P. Mansfield, *J. Phys. C Solid State Phys.* **4**, 1444–1452 (1971).
3. L. M. K. Vandersypen, I. L. Chuang, *Rev. Mod. Phys.* **76**, 1037–1069 (2005).
4. H. Zhou et al., *Phys. Rev. X* **10**, 031003 (2020).
5. T. Oka, S. Kitamura, *Annu. Rev. Condens. Matter Phys.* **10**, 387–408 (2019).
6. A. C. Potter, T. Morimoto, A. Vishwanath, *Phys. Rev. X* **6**, 041001 (2016).

7. F. Nathan, D. Abanin, E. Berg, N. H. Lindner, M. S. Rudner, *Phys. Rev. B* **99**, 195133 (2019).
 8. D. V. Else, B. Bauer, C. Nayak, *Phys. Rev. Lett.* **117**, 090402 (2016).
 9. N. Y. Yao, A. C. Potter, I.-D. Potirniche, A. Vishwanath, *Phys. Rev. Lett.* **118**, 030401 (2017).
 10. S. Choi *et al.*, *Nature* **543**, 221–225 (2017).
 11. J. Zhang *et al.*, *Nature* **543**, 217–220 (2017).
 12. J. Rovny, R. L. Blum, S. E. Barrett, *Phys. Rev. Lett.* **120**, 180603 (2018).
 13. J. Smits, L. Liao, H. T. C. Stoof, P. van der Straten, *Phys. Rev. Lett.* **121**, 185301 (2018).
 14. Z. Gong, R. Hamazaki, M. Ueda, *Phys. Rev. Lett.* **120**, 040404 (2018).
 15. N. Y. Yao, C. Nayak, L. Balents, M. P. Zaletel, *Nat. Phys.* **16**, 438–447 (2020).
 16. L. D'Alessio, M. Rigol, *Phys. Rev. X* **4**, 041048 (2014).
 17. D. A. Abanin, E. Altman, I. Bloch, M. Serbyn, *Rev. Mod. Phys.* **91**, 021001 (2019).
 18. N. Y. Yao *et al.*, *Phys. Rev. Lett.* **113**, 243002 (2014).
 19. W. De Roeck, F. Huveneers, *Phys. Rev. B* **95**, 155129 (2017).
 20. S. Autti, V. B. Eltsov, G. E. Volovik, *Phys. Rev. Lett.* **120**, 215301 (2018).
 21. K. Giergiel *et al.*, *New J. Phys.* **22**, 085004 (2020).
 22. S. Autti *et al.*, *Nat. Mater.* **20**, 171–174 (2021).
 23. D. V. Else, C. Monroe, C. Nayak, N. Y. Yao, *Annu. Rev. Condens. Matter Phys.* **11**, 467–499 (2020).
 24. T. Kuwahara, T. Mori, K. Saito, *Ann. Phys.* **367**, 96–124 (2016).
 25. D. A. Abanin, W. De Roeck, W. W. Ho, F. Huveneers, *Phys. Rev. B* **95**, 014112 (2017).
 26. F. Machado, G. D. Kahanamoku-Meyer, D. V. Else, C. Nayak, N. Y. Yao, *Phys. Rev. Research* **1**, 033202 (2019).
 27. A. Rubio-Abadal *et al.*, *Phys. Rev. X* **10**, 021044 (2020).
 28. P. Peng, C. Yin, X. Huang, C. Ramanathan, P. Cappellaro, *Nat. Phys.* **17**, 444–447 (2021).
 29. D. V. Else, B. Bauer, C. Nayak, *Phys. Rev. X* **7**, 011026 (2017).
 30. F. Machado, D. V. Else, G. D. Kahanamoku-Meyer, C. Nayak, N. Y. Yao, *Phys. Rev. X* **10**, 011043 (2020).
 31. V. Khemani, R. Moessner, S. L. Sondhi, A Brief History of Time Crystals. [arXiv:1910.10745](https://arxiv.org/abs/1910.10745) [cond-mat.str-el] (23 October 2019).
 32. L. Landau, *Zh. Eksp. Teor. Fiz.* **7**, 19–32 (1937).
 33. A. Sørensen, K. Mølmer, *Phys. Rev. Lett.* **82**, 1971–1974 (1999).
 34. See supplementary materials.
 35. C. Monroe *et al.*, Programmable Quantum Simulations of Spin Systems with Trapped Ions. [arXiv:1912.07845](https://arxiv.org/abs/1912.07845) [quant-ph] (29 July 2020).
 36. D. V. Else, W. W. Ho, P. T. Dumitrescu, *Phys. Rev. X* **10**, 021032 (2020).
 37. I.-D. Potirniche, A. C. Potter, M. Schleier-Smith, A. Vishwanath, N. Y. Yao, *Phys. Rev. Lett.* **119**, 123601 (2017).
 38. D. V. Else, P. Fendley, J. Kemp, C. Nayak, *Phys. Rev. X* **7**, 041062 (2017).
 39. S. Choi, N. Y. Yao, M. D. Lukin, Quantum metrology based on strongly correlated matter. [arXiv:1801.00042](https://arxiv.org/abs/1801.00042) [quant-ph] (29 December 2017).
- ACKNOWLEDGMENTS**
We acknowledge fruitful discussions with C. Laumann, W. L. Tan, A. Vishwanath, D. Weld, and J. Zhang. **Funding:** This work is supported by the DARPA Driven and Nonequilibrium Quantum Systems (DRINQS) program D18AC00033; the NSF Practical Fully-Connected Quantum Computer program PHY-1818914; the DOE Basic Energy Sciences: Materials and Chemical Sciences for Quantum Information Science program DE-SC0019449; the DOE High Energy Physics: Quantum Information Science Enabled Discovery Programs DE-0001893; the AFOSR MURI on Dissipation Engineering in Open Quantum Systems FA9550-19-1-0399; the David and Lucile Packard foundation; the W. M. Keck foundation; and the EPIQS Initiative of the Gordon and Betty Moore Foundation, GBMF4303. **Author contributions:** A.K., W.M., P.B., K.S.C., L.F., P.W.H., G.P., and C.M. designed and performed experimental research; F.M., D.V.E., C.N., and N.Y.Y. analyzed the data theoretically; and all authors wrote the paper. **Competing interests:** C.M. is the cofounder and chief scientist at IonQ, Inc. The authors declare no other competing interests. **Data and materials availability:** All data needed to evaluate the conclusions in the paper are present in the paper or the supplementary materials.
- SUPPLEMENTARY MATERIALS**
science.sciencemag.org/content/372/6547/1192/suppl/DC1
Supplementary Text
Figs. S1 to S6
References (40–47)
- 28 January 2021; accepted 30 April 2021
10.1126/science.abg8102